COMPUTATIONAL ANALYSIS OF PROPELLER SLIPSTREAM AERODYNAMIC EFFECTS

JELENA SVORCAN

University of Belgrade, Faculty of Mechanical Engineering, Belgrade, Serbia, jsvorcan@mas.bg.ac.rs

OGNJEN PEKOVIĆ

University of Belgrade, Faculty of Mechanical Engineering, Belgrade, Serbia, opekovic@mas.bg.ac.rs

TONI IVANOV

University of Belgrade, Faculty of Mechanical Engineering, Belgrade, Serbia, tivanov@mas.bg.ac.rs

MARIJA BALTIĆ

University of Belgrade, Faculty of Mechanical Engineering, Belgrade, Serbia, mbaltic@mas.bg.ac.rs

Abstract: *Numerical investigation of a representative (turboprop commuter) propeller slipstream aerodynamic effects on different nacelle/wing combinations is performed in a commercial software package ANSYS FLUENT. The obtained numerical results are compared to the experimental values of pressure coefficient obtained in a low speed wind tunnel investigation. The study is performed for two reasons: i) to gain more physical insight into the complex flow field that consequently appears, and ii) to evaluate the chosen software and test its abilities to adequately represent this unsteady, three-dimensional, rotational, interacting flow field. In the presented numerical study, flow field is computed by Unsteady Reynolds Averaged Navier-Stokes (URANS) equations closed by 2-equation k-ω SST turbulence model. Presented results include fluid flow visualizations in the form of pressure coefficient and vorticity contours and the values of aerodynamic coefficients.*

Keywords: *propeller, slipstream, aerodynamic performance, RANS.*

1. INTRODUCTION

Since propelled flight is efficient, it has often been the topic of numerous aerodynamic investigations (both experimental and computational) as well optimization studies [1-9]. One of its most interesting and significant flow phenomena is the spiraling slipstream that appears as a consequence of the rotating surfaces (blades) generating and shedding vortices. It can produce considerable (un)favorable effects (e.g. side forces, yaw moments) on the latter aerodynamic surfaces. Complete aerodynamic analysis is complex and highly depends on the lift distribution, geometry, flow conditions, etc. Although fundamental computational model based on Momentum and Blade Element Theory is nearly 100 years old, it is still most usually employed for its simplicity and satisfactory accuracy. However, if one is concerned with the complete flow field, more advanced numerical simulations (usually in the form of finite volume method applied to RANS equations) are also an accessible tool [5, 6, 8] whose accuracy should be validated, i.e. compared to experimental data.

Apart from large scale geometries, nowadays, small unmanned air vehicles also interest scientific population, and there are many examples of such vehicles employing a propeller (or a rotor, or a tilted rotor) [8, 9]. Therefore, the effect of the propeller on the rest of the aircraft is important for flight performance, particularly at high angles-of-attack of high pitch (and roll and yaw) rates.

Propellers incorporate all the complex characteristics of wind turbine and helicopter blades. Their tip speed is high, with compressibility effects present (similar to helicopter blades), while their geometry is quite curved and convoluted (reminiscing wind turbine blades). Geometrically, aspect ratio of propeller blades *AR* is high, while chord and twist distributions are non-linear. For those reasons, main motivation of the study is to inspect (investigate) the surrounding complex rotational flow and its effects on accompanying aerodynamic surfaces.

Additional complications to simulating flow around propellers originate from the fact their performances change with different collective pitch and tip-speed ratio (since these parameters define the velocity triangle each blade segment is subjected to). For accurate estimation of propeller flight performances it is necessary to know the complete map of its aerodynamic characteristics. On the other hand, propeller geometry is usually commercial, and not freely available. Experimental results are incomplete, rare, old or inaccessible. Trustworthy comparisons between experimental and numerical data are difficult to perform.

The paper deals with and presents results of numerous computed flow cases. Unfortunately, due to the lack of actual geometrical data of the propeller, the study is of a more qualitative type. It is divided into two parts: the first deals with the fluid flow around a stand-alone propeller (similar to [3, 4]),

and the second with the effect of that propeller onto two different fuselage/wing configurations [1, 2].

2. MODEL PROPELLER

Since the original geometry of the propeller used in [1, 2] is unavailable, a "comparable" model was adopted, approach similar to [3].

The geometry used in this study is derived from 1/5th scale model of the 4-bladed Dowty Rotol R212 propeller [4]. Propeller model diameter equals $D = 0.732$ m. Approximated thickness, chord and twist distributions are illustrated in Fig. 1. Sectional values are marked with a square marker.
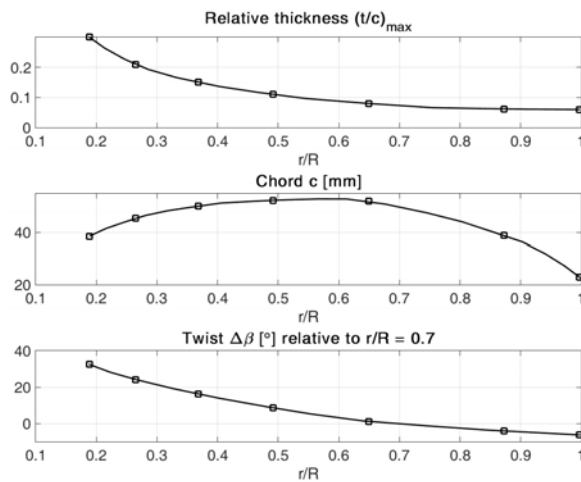
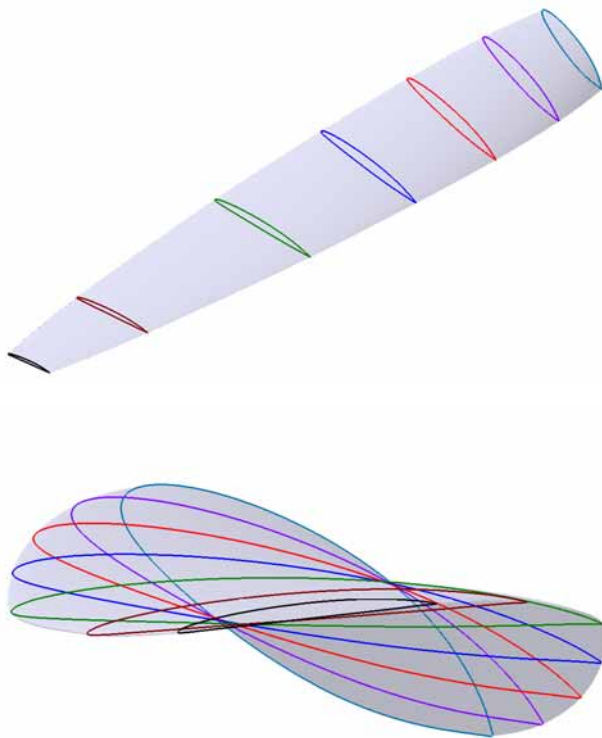**Figure 1.** Blade spanwise characteristics

Figure 2. Blade model

Airfoils employed along the blade belong to NACA 16-series, derived for use at high speeds, particularly for propeller applications [10]. However, the work presented in [4] does not state which particular airfoils were used, uncambered or cambered (and how much). Therefore, three airfoil families were chosen and investigated in more detail: NACA 16-0XX, NACA 16-5XX and NACA 16-10XX. The third (and fourth) digit indicates the amount of camber in the form of design lift coefficient (here $C_L = 0$, 0.5 or 1.0), i.e. the camber line is the same for all airfoils of one family. According to the standard notation, the final two digits XX express the airfoil thickness that varies along the blade.

Airfoils of NACA 16-5XX series distributed along the blade are presented in Fig. 2 for comparison and illustration.

2.1. Geometrical model

The propeller consists of four blades with a blunt trailing edge. Only the streamlined part of the blade surface is modeled, approximately in the range $0.19 < r/R < 0.99$, Fig. 2. Rotor (rotational part around the blades) is shaped like a cylinder. Distance from the blades in every direction is 0.1 m. Stator (stationary control volume) is also in the form of a cylinder stretching +1.5 m before and −3 m after the blades, and 1.5 m radially from the blades. Percentually, the rotor area constitutes less than 3.5 % of the total stator cross-section, thereby imitating the wind tunnel measurement.

Computational meshes are hybrid unstructured with the boundary layer encompassing the blades (first layer thickness $y_1 = 0.02$ mm, maximum number of layers $N = 25$, growth rate $q = 1.2$). Sizing functions ensuring sufficient levels of grid quality (results independence) are defined along the blade surface (grid convergence study is performed). Final meshes comprise approximately 2.5 million cells.

2.2. Experimental and numerical simulation of an isolated propeller

All the necessary data on the performed measurements can be found in [4]. Experiments were performed in RAE 1.5 m acoustic tunnel. Propeller power absorption and thrust have been measured over a range of rotational speeds up to 8000 rpm with mainstream air speed varied from $U_0 = 15$ to 57.5 m/s. Tests were performed over several different blade settings (pitch angles), namely $\beta_{0.7} = [9.3°, 17.3°, 22.4°, 27.3°, 34.9°]$.

Numerical simulations were performed in ANSYS FLUENT where governing flow equations for viscous fluid are solved by finite-volume method. Given the small flow velocity, $U_0 = 50$ m/s, and small propeller diameter (resulting in relative tip velocity not greater than 150 m/s) pressure-based incompressible solver was used. Density based solver (with energy and ideal-gas equations on) was also tried, but since the difference in the two sets of results was negligible, the former approach was applied in the remainder of the presented study.

Air is considered as incompressible fluid of constant viscosity while the flow is steady. k-ω SST turbulence model is employed for the closure of RANS equations describing the fluid flow. Rotor rotation is simulated by the

moving frame of reference (steady) approach. No-slip boundary conditions were assigned to all wall surfaces, while Dirichlet boundary conditions concerning velocity and pressure were imposed on the inlet and outlet surfaces.

Pressure-velocity coupling was resolved by a more stable SIMPLEC scheme. Gradients were obtained by the least squares cell-based method. Spatial discretizations were 2nd order. Computations were performed until fluctuations of aerodynamic coefficients became negligible, usually around 1000 iterations.

2.3. Aerodynamic performance

Numerous simulations had to be performed to determine the correct airfoil series used in the experimental model. The values of power and thrust coefficients are computed from values of total torque (from tangential force) and normal force acting on all four blades:

$$C_T = \frac{T}{\rho n^2 D^4}, C_P = \frac{P}{\rho n^3 D^5} \qquad (1)$$

where n is rotational frequency in [Hz]. Dimensionless velocity, i.e. advance ratio, is computed as:

$$J = \frac{U_0}{nD} \qquad (2)$$

Comparisons of computed thrust and power coefficients and efficiency

$$\eta = \frac{C_T J}{C_P} \qquad (3)$$

as functions of advance ratio to experimental values are presented in Figs. 3-5. Overall, the correspondence between the two sets of results is satisfactory. It can be concluded that the airfoils of the tested blade mostly resemble NACA 16-5XX series airfoils that were used in the remainder of the study.
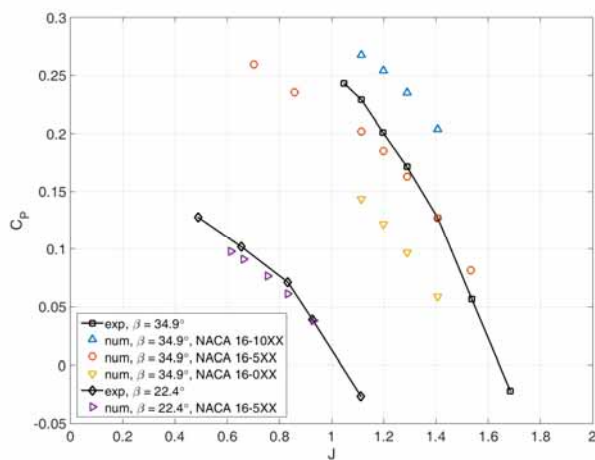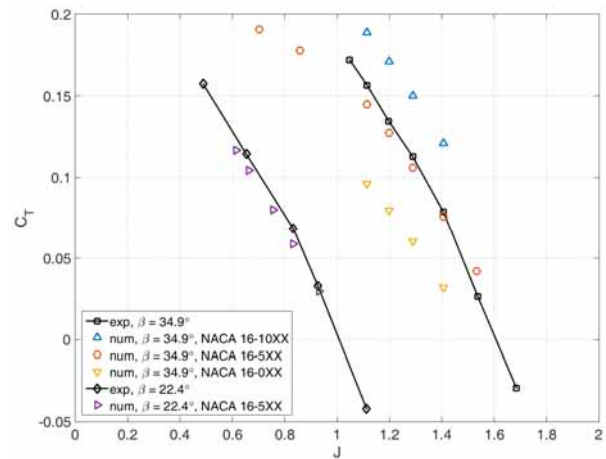

Figure 3. Power coefficient C_P
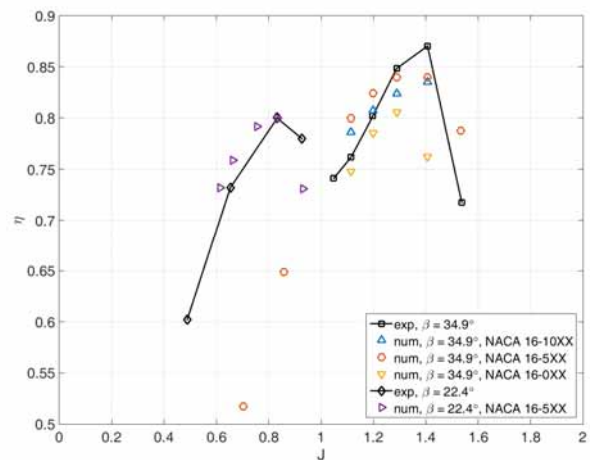

Figure 4. Thrust coefficient C_T

Figure 5. Efficiency η

3. DESCRIPTION OF THE PROPELLER − NACELLE/WING COMBINATIONS

3.1. Geometry and experimental testing

This part of the study relies on the experimental data obtained in the mid-1980s by FFA, the Aeronautical Research Institute of Sweden. Detailed description of experimental set-up can be found in [1, 2].

Two different nacelle/wing configurations (of available four) were chosen for numerical investigation. The first is composed from the model propeller and an axisymmetrical nacelle whose coordinates can be found in [1]. The second one is derived from the 1st supplemented with an unswept rectangular wing whose span is $b = 2$ m, and chord $c = 0.5$ m. Reference area is $S = 1.672$ m^2. Used airfoil section is symmetric NACA $63_{(10)}$A-012. Figure 6 illustrates the two configurations, with adopted coordinate system, reference point location and global dimensions.

3.2. Numerical simulations

Model geometry is constructed according to the tested one (rigid wall surfaces are: *spinner*, *blades*, *nacelle*, *base*, *wing*). The rotational part is similar in size to the cylinder

used in the propeller stand-alone simulations, but now contains two rotating surfaces: *blades* and parabolic *spinner*. Stator is again in the form of a cylinder stretching approximately +1.5 m before and −3 m after the blades, and 1.5 m radially from the blades. The non-rotating surfaces are: *nacelle*, *base* (and *wing* in Configuration 2).
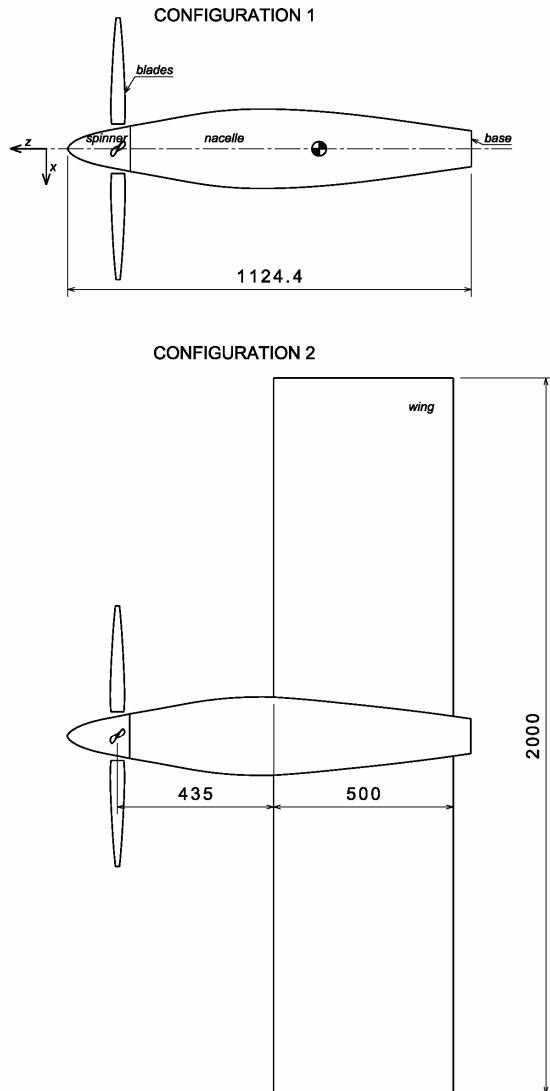

Figure 6. Propeller − nacelle/wing configurations

Computational meshes are hybrid unstructured with the boundary layer encompassing the *spinner* and *blades* ($y_1 = 0.02$ mm, $N = 20$, $q = 1.2$) and the *nacelle*, *base* and *wing* ($y_1 = 0.1$ mm, $N = 10$, $q = 1.2$). Sizing functions ensuring sufficient levels of grid quality are defined along the *blade* and *spinner* surfaces as well as stationary surfaces. Final meshes for Configuration 1 and 2 contain approximately 4 and 5 million cells, respectively.

Again, for simplicity, pressure-based solver assuming incompressible fluid is used and numerical set-up is similar to the previously mentioned one. However, given non-zero angles-of-attack (and deviation from axisymmetric flow case), the flow had to be simulated as transient with *sliding mesh* approach employed. The simulations lasted for 3 rotations until quasi-convergence was achieved. Time-step corresponds to the angular increment of 5°, i.e. d$t = T/72$, where $T = 2\pi n$.

4. RESULTS AND DISCUSSION

The two configurations were tested/simulated at different angles-of-attack α (lying in yz-plane) with propeller rotating or standing still (on or off notation in diagrams). The boundary/operating conditions of a working propeller are:
- $U_0 = 50$ m/s,
- $n = 5825$ rpm,
- $\beta_{0.7} = 34.9°$,
- $C_T = 0.220$,
- $C_P = 0.277$,
- $\eta = 0.560$.

The propeller rotates in the clockwise direction.

4.1. Configuration 1

Pressure coefficient contours along wall surfaces obtained at three different angles-of-attack $\alpha = [0°, 5°, 10°]$ with a working propeller are presented in Fig. 7. Due to axisymmetric geometry the flow at zero AoA is also nearly axisymmetric, Fig. 7a. Some discrepancies appear near the slots between the spinner and the blades (which is a consequence of the modified propeller geometry).
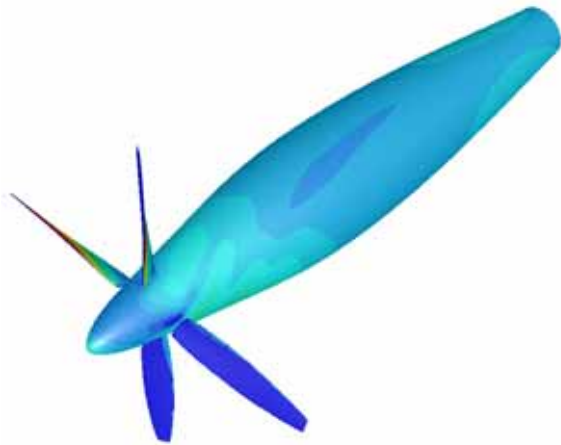
Induced flow is apparent at the front of the nacelle, but it slowly dies out towards the base surface.
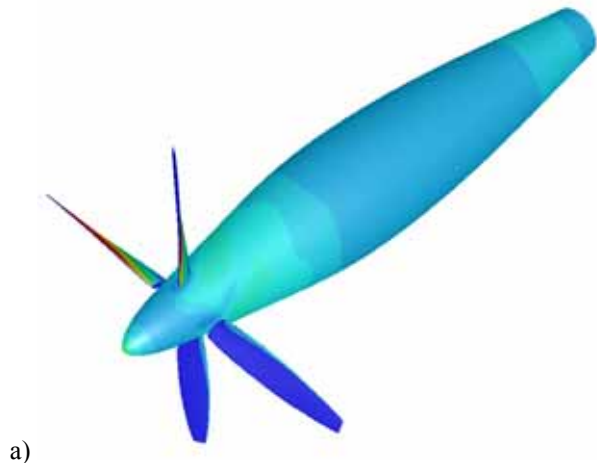
a)
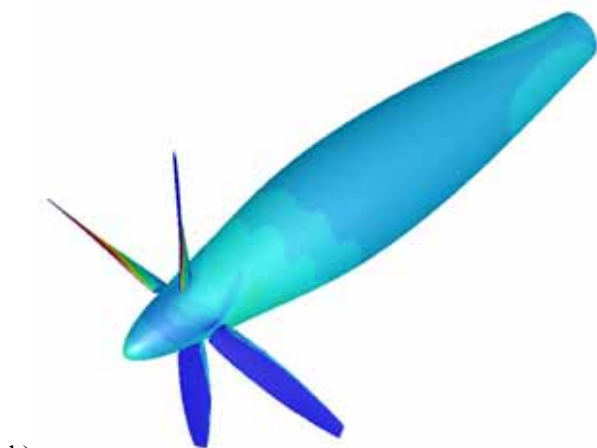
b)

c)

Figure 7. Pressure coefficient contours along wall surfaces at: a) $\alpha = 0°$, b) $\alpha = 5°$ and c) $\alpha = 10°$

At higher AoAs, the flow is distinctly unsymmetrical (pressure is higher at the left half of the model) with the appearance of the side force.

Although some discrepancies between models exist, computed aerodynamic force and moment coefficients acting only on the *nacelle* are compared to experimental values, Fig. 8, for a rotating and non-moving propeller. C_x corresponds to the side force, C_y to normal and C_z to axial force, while C_l and C_m match pitching and yawing moments, respectively. The correspondence between experimental and computational data is satisfactory.
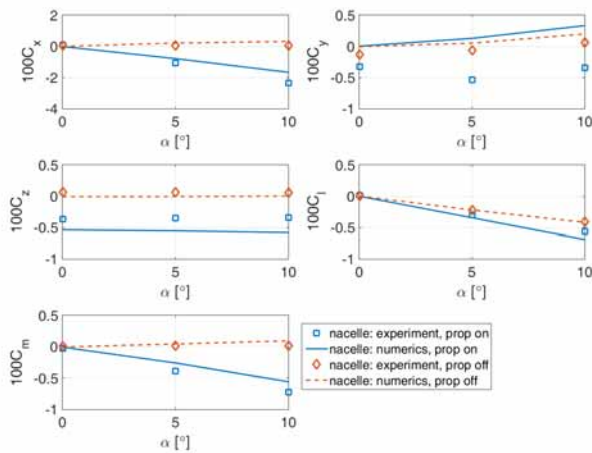

Figure 8. Coefficients of forces and moments acting on *nacelle* in Configuration 1

4.2. Configuration 2

Pressure coefficient distributions along the wall surfaces of Configuration 2 at different AoAs with a rotating propeller are presented in Fig. 9. The existence of wing clearly affects the pressure distribution along the nacelle (straightening effect at higher AoAs).

Chord- and spanwise wing surface pressure distributions can also be deduced from Fig. 9. On the part of the wing surface behind the rotor there is strong flow asymmetry (both between the upper and lower wing surfaces, as well as the left and right half wing). At higher AoAs, there is significant rolling moment. Right wing-half is generating more lift as is illustrated in Fig. 10.
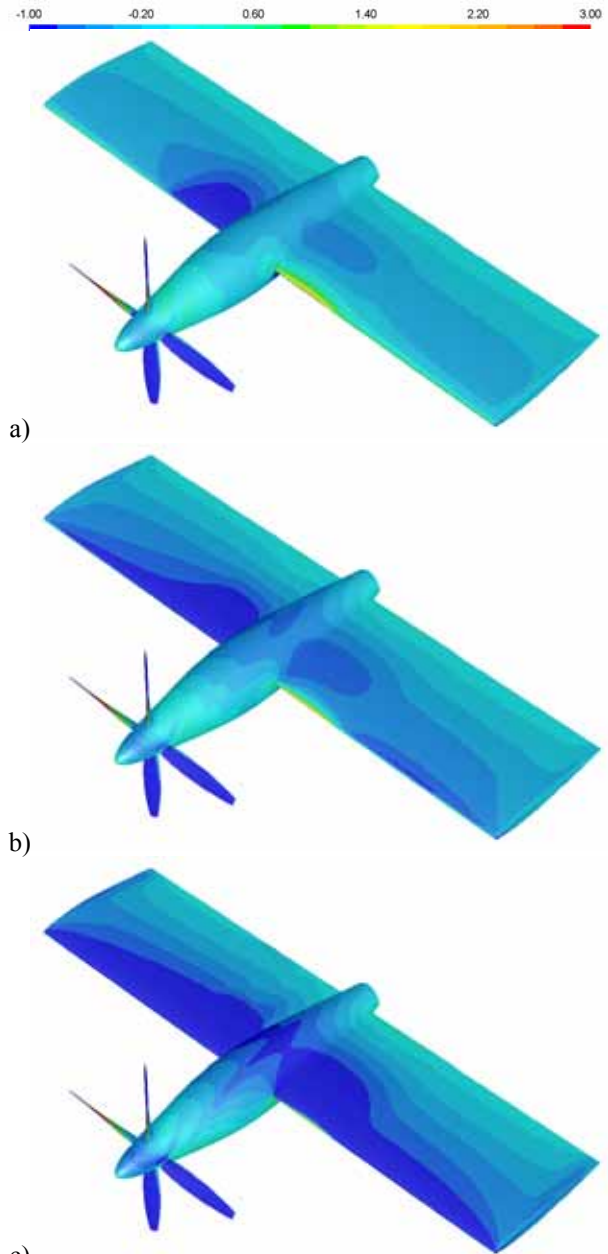
a)

b)

c)

Figure 9. Pressure coefficient contours along wall surfaces at: a) $\alpha = 0°$, b) $\alpha = 5°$ and c) $\alpha = 10°$
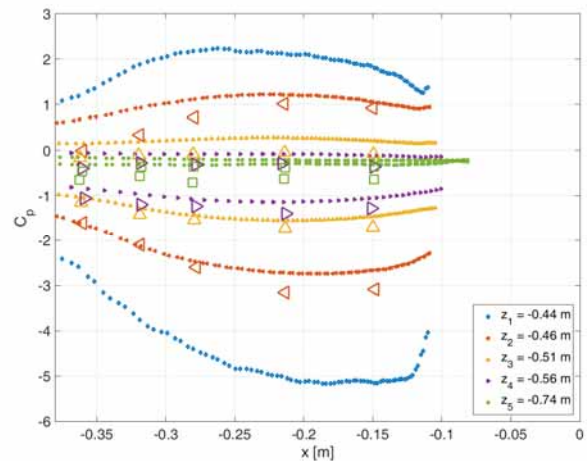

Figure 10. Spanwise pressure coefficient distributions along the right wing-half

Flow features can be depicted by vorticity contours around the model, Fig. 11. Again, asymmetric, rotational flow is clearly visible.
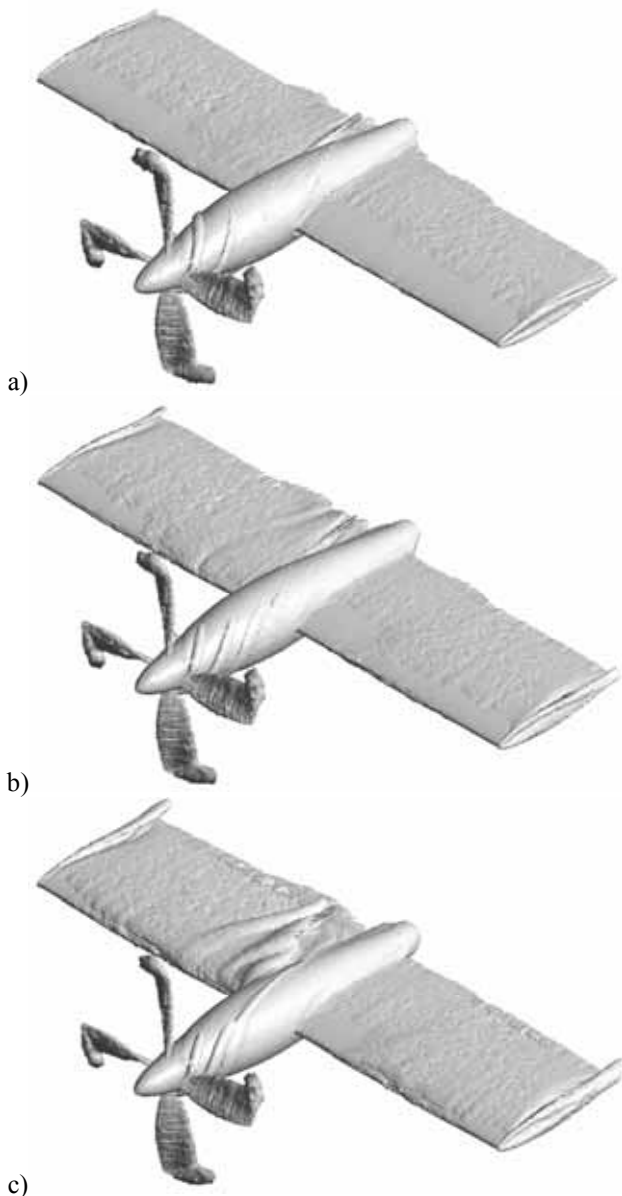

a)

b)

c)

Figure 11. Vorticity contours around the Configuration 2 at: a) $\alpha = 0°$, b) $\alpha = 5°$ and c) $\alpha = 10°$

5. CONCLUSIONS

Transient, 3D simulations of the viscous flow around an isolated propeller as well as the one accompanied by different nacelle/wing configurations have been conducted. Results are numerous and could not be presented in whole. The paper exhibits only a small amount of obtained data in the form of pressure and vorticity distributions.

Comparisons to available experimental data have been made. Although there are some differences in used geometries, and the study is primarily qualitative, the two sets of results correspond well. Flow physics has been captured; the increments in forces and moments with varying AoA have been documented and distinguishing flow features have been illustrated.

The study validates and justifies the use of a more complex computational model since the amount and quality of the obtained data are satisfactory.

ACKNOWLEDGEMENT

References

[1] Samuelsson, I., *Low speed wind tunnel investigation of propeller slipstream aerodynamic effects on different nacelle/wing combinations, Part 1*, FFA TN 1987-22, The Aeronautical Research, Institute of Sweden, 1987.

[2] Samuelsson, I., *Low speed wind tunnel investigation of propeller slipstream aerodynamic effects on different nacelle/wing combinations, Part 2*, FFA TN 1990-24, The Aeronautical Research, Institute of Sweden, 1991.

[3] Strash, D. J., Lednicer, D. A., Rubin, T. D., "Analysis of propeller-induced aerodynamic effects", 16th AIAA Applied Aerodynamics Conference, 15-18 June 1998, Albuquerque, N.M., U.S.A.

[4] Trebble, W. J. G., "Investigation of the aerodynamic performance and noise characteristics of a 1/5th scale model of the Dowty Rotol R212 propeller", Aeronautical Journal, May (1987), pp. 225-36.

[5] Ghoddoussi, A., *A more comprehensive database for propeller performance validations at low Reynolds numbers*, Ph. D. Thesis, Department of Aerospace Engineering, Graduate School of Wichita State University, Ks., U.S.A., 2016.

[6] Della Vecchia, P., Malgieri, D., Nicolosi, F., De Marco, A., "Numerical analysis of propeller effects on wing aerodynamic: tip mounted and distributed propulsion", Transportation Research Procedia, 29 (2018), pp. 106-115.

[7] Catalano, F. M., "On the effects of an installed propeller slipstream on wing aerodynamic characteristics", Acta Polytechnica, 44(3) (2004), pp. 8-14.

[8] Ning, Z., Hu, H., "An experimental study on the aerodynamics and aeroacoustic characteristics of small propellers of UAV", AIAA SciTech Forum, 4-8 January 2016, San Diego, Cal., U.S.A.

[9] Dimchev, M., *Experimental and numerical study on wingtip mounted propellers for low aspect ratio UAV design*, M. Sc. Thesis, Faculty of Aerospace Engineering, Delft University of Technology, Netherlands, 2012.

[10] Lindsey, W. F., Stevenson, D. B., Daley, B. N., *Aerodynamic characteristics of 24 NACA 16-series airfoils at Mach numbers between 0.3 and 0.8*, NACA TN 1546, Langley Aeronautical Laboratory, Langley Field, Va., 1948.